Analytical Methods

Accepted Manuscript

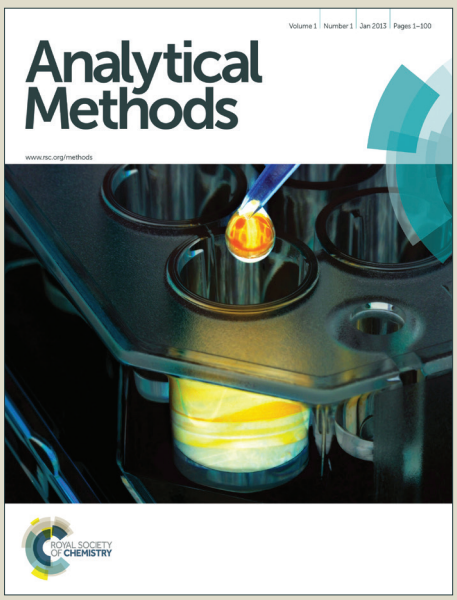

ROYAL SOCIETY OF CHEMISTRY

www.rsc.org/methods

Electrodeposition of prussian blue nanoparticles on polyaniline coated halloysite nanotubes for nonenzymatic hydrogen peroxide sensing

Qinglin Sheng, Dan Zhang, Qian Wu, Jianbin Zheng*, Hongsheng Tang

Institute of Analytical Science, Shaanxi Provincial Key Laboratory of Electroanalytical Chemistry, Northwest University, Xi'an, Shaanxi 710069, China

Abstract:

A facile and effective electrochemical sensing technique was developed by the electrodeposition of prussian blue on polyaniline (PANI) coated halloysite nanotubes (HNTs). Owing to the special structure of the PB-PANI-HNTs nanocomposite, the sensor possessed excellent electrocatalytic ability towards H_2O_2 reduction. The amperometric study demonstrated the H_2O_2 sensor possess well performance with a linearity in the range from 4 μM to 1064 μM. The limit of detection (LOD) was 0.226 μM (S/N=3) and the sensitivity was calculated to be 0.98 μA/ (μM·cm^2). Moreover, the interference from the common interfering species such as glucose, ascorbic acid, dopamine and uric acid can be effectively avoided, and the sensors exhibit long-term stability, thus holding promise for the development of amperometric biosensors.

Key words: Prussian blue, Halloysite nanotubes, Polyaniline, nonenzymatic, Sensor

*Corresponding author. Tel.: +86-29-88302077; Fax: +86-29-88303448.

E-mail address: zhengjb@nwu.edu.cn (J. B. Zheng).

1. Introduction

Hydrogen peroxide (H_2O_2) is an essential mediator with wide use such as biology,[1-2] clinical control[3] and environmental protection[4] and so on. Therefore the determination of H_2O_2 is of great importance. Although various techniques have been found to detect H_2O_2, including fluorimetry,[5] titrimetry,[6] chemiluminecence,[7] electrochemical sensors,[8] among all these approaches, electrochemical techniques are the powerful methods for the detection of analytes due to their particular characteristics comparing to other techniques for monitoring of H_2O_2 such as high sensitivity, selectivity, and simplicity.[9]

Prussian blue (PB) is well known as one of the first reported mixed-valence transition metal hexacyanometalates with the formula of $Fe_4^{III}[Fe^{II}(CN)_6]_3$.[10] The peculiar characteristics of the reduced form of PB, Prussian white (PW), is able to catalyze the electrochemical reduction of hydrogen peroxide at low potentials,[11] and this is crucial for the application of a biosensor in real samples avoiding the interference from coexisting substances (such as glucose, ascorbic acid, uric acid, among several others).[12-13] Its high electrocatalytic activity and selectivity toward the reduction of hydrogen peroxide (H_2O_2) make it an "artificial peroxidase".[14] PB also presents very interesting electrochromic behavior (it becomes colorless when reduced to the so-called Prussian white and pale green when oxidized to the so-called Berlin green structure).[15] It is widely applied to fabricate H_2O_2 sensor since the development of highly sensitive and interference-free H_2O_2 amperometric sensors.

Various ways have been involved in the fabrication of PB-based hybrids with different, [16-18] while the well control over size and shape of prussian blue nanoparticles is still a challenge. More efforts are still needed to design novel PB based hybrids and develop simple preparation methods. Electrochemical deposition of PB is widely used for fabrication of PB-modified electrode due to its

controllable and rapid preparation. However, the lower electrochemical stability of the PB thin film and its easy leakage from the surface of the electrode seriously restrain the further application and development to sensors.[19] Hence, searching for a desirable active support is crucial to improve the electrochemical stability thus avoiding the leaching of PB.[20-21] The support can not only acts as a carrier of the active components but also contributes a lot to the activity of the nanoparticles. Recently, nanotubes have been widely used to support nanocomposite.[22]

Halloysite nanotubes (HNTs) as novel kind of natural nanotubes have been acknowledged as a rising star in the area of material science due to their high porosity, abundance in nature, non-toxic and low cost,[23] they are naturally occurring aluminosilicates ($Al_2Si_2O_5(OH)_4 \cdot nH_2O$) with a regular nanotubular bulk structure, morphology, rich mesopores and nanopores.[24] Typically, the inner diameter, outer diameter and length of the tubes are about 1-30 nm, 30-50 nm and 100-2000 nm, respectively, which allows metal particles to be fixed on the out surface or the inner tube preparing highly efficient metal-supported catalysts.[25] Moreover, the nanolumen structures always could be a natural barrier for the diffusions of reactants, which may enhance the catalytic rate. Compared to carbon nanotubes (CNTs), HNTs were selected as reliable substrates in many scopes due to their unique characteristics, such as different outside and inside chemistry and adequate hydroxyl groups on the surface of HNTs.[26] Therefore, halloysites are of great potential applications in industrial catalytic systems. Moreover, conducting polymer nanotubes composites have received significant interest because the incorporation of nanotubes in conducting polymers can lead to new composite materials possessing the properties of each component with synergistic effects that would be useful in particular applications.[27] Polyaniline as a typical conducting polymer make it a best choose to modified HNTs and then to deposite PB nanoparticles on the surface of PANI-HNTs. To the best of

our knowledge, little attention has been paid to the application of halloysite nanotubes in PB based hybrids.

In this investigation, we reported the coating of polyaniline onto the surfaces of the halloysite nanotubes via the one-step in situ polymerization, and then PB nanoparticles were electrodeposited on the surface of PANI-HNTs/GCE under the protection of PVP. Consequently, a sensitive method for H_2O_2 detection was developed as the schematic illustration shown in Fig. 1. The morphology of the nanocomposite was characterized by transmission electron microscopy. The activity of the PB-PANI-HNTs modified glassy carbon electrode toward the electrochemical reduction of H_2O_2 with emphasis on the high sensitivity of the electrode is studied. Cyclic voltammetry (CV) and amperometry techniques were used in the investigation of H_2O_2 reduction on PB-PANI-HNTs. In addition the detection limit, linear range, selectivity and stability are further investigated.

Fig. 1

2. Experimental

2.1. Chemicals and Apparatus

Halloysite nanotubes were purchased from Natural Nano. Inc. Ferric chloride ($FeCl_3 \cdot 6H_2O$), potassium ferricyanide ($K_3Fe(CN)_6$), potassium chloride (KCl), hydrochloric acid(HCl, 12 M) were purchased from Xi'an Chemical Reagent (Xi'an, China). Hydrogen peroxide (30%), Aniline, Ammonium persulfate ($(NH_4)_2S_2O_8$, APS, 98%), PVP (K30) were purchased from purchased from Tianjin Tianli Chemistry Reagent Co., Ltd (Tianjin, China). All aqueous solutions were prepared using deionized water (Milli-Q system).

The transmission electron microscope (TEM) and energy-dispersed spectrum (EDS) were observed were done on a JEM-2100 scanning electron microscope (JEOL, Japan). FTIR was carried

out by A Bruker Tensor 27 FTIR spectrometer. All electrochemical measurements were carried out by a CHI660 electrochemical workstation (CH Instruments, Shanghai, China) with a conventional three-electrode system, a bare or modified glassy carbon electrode (3 mm in diameter, GCE), a platinum wire, and a saturated calomel electrode (SCE) were used as the working electrode, counter electrode and reference electrode respectively.

2.2. Synthesis of PANI-HNTs composite

The PANI-HNTs nanocomposites were synthesized by one-step in situ polymerization of aniline in the presence of HNTs. Ammonium persulfate (APS) was used as an oxidant. A description of the synthesis method is given as follows. 100 mg of HNTs was dispersed in 50 mL solution containing 1 M HCl, followed with successive sonication at room temperature for 1 h. Then, 0.5 mL of anline monomer was added to the above suspension and was stirred for 1 h. After that, 1 M HCl solution containing 0.45 g of APS was added to the reaction mixture drop by drop slowly. The polymerization of aniline occurred when the suspension turned to dark green, after which the solution were kept at room temperature and left at rest to polymerize for another 4 h. Then the PANI-HNTs nanostructures were collected by centrifuge after being washed several times with DIW and alcohol and then dried under vacuum at 80 °C overnight. Lastly, 10 mg of thus prepared PANI-HNTs is dispersed in 10 mL ethanol.

2.3. Synthesis of PB-PANI-HNTs

Before modification, the glassy carbon electrodes (GCEs) was carefully polished with mirror finish by using alumina in water slurry and washed with deionized water. It was further cleaned by sonication successively in 1:1 nitric acid, absolute alcohol, and doubly distilled water, then dry in a stream of nitrogen for modification. Then, drop-casting technique is used to get PANI-HNTs on

glass carbon electrode. 10 μL of the PANI-HNTs were coated on the GCE and dried at 60 °C for next use.

Typically, electrochemical deposition is applied to get PB-PANI-HNTs films under the protection of PVP. The as-prepared PANI-HNTs modified GCE was cycled between -0.2 V to 1.2 V at room temperature (approximately 25 °C) with a scan rate of 50 mV $\cdot s^{-1}$ for 10 cycles in an oxygen-free solution containing 1 mM of $FeCl_3$ and 1 mM of $[K_3Fe(CN)_6]$, 0.025 M of HCl and 0.1 M of KCl were used as the supporting electrolyte, additionally, PVP was also used to protect PBNPs onto the modified electrode. After rinsing with double-distilled water, the PBNPs-PANI-HNTs modified electrode was dried in air and later under the infrared lamp for approximately 2 h allowing the so-called zeolitic water removed from the PBNPs irreversibly.[28]

The cyclic voltammetric process of the electrodeposition process was investigated. Results showed that the peak current of cathodic and anodic waves increased gradually as the cycles increase owing to the increase of PB loadings. The current both tend to be stable after ten cycles, illustrating electroposition of PB is almost completed. Moreover, a PB/GCE was prepared by electrodepositing PBNPs on a glassy carbon electrode in the same conditions for comparison.

3. Results and discussion

3.1. Characterization of the PB-PANI-HNTs

Fig. 2

The detailed morphological and structural features of HNTs and the prepared PANI-HNTs PB-PANI-HNTs were investigated by TEM (Fig. 2). Fig. 2A and Fig. 2B show the structure and morphology of HNTs, the HNTs are about 70 nm in diameter and present obvious hollow structure

after the polymerization of PANI, the whole HNT has been entrapped in the PANI film as shown in Fig. 2C and Fig. 2D, the composite is typical core-shell structures in which the HNT serves as the core and is dispersed individually into the PANI matrix. The rough surface and the large surface area of the PANI-HNTs provided more sites for the deposition of prussian blue nanoparticles. From Fig. 2E and F, it can be seen that PB is uniformly deposited on the surface of PANI-HNTs with the diameter nanoscaled, few accumulation of the PBNPs can be found, indicating the electrochemically synthesis of PVP protected PBNPs is applicable. The energy dispersive spectroscopy (EDS) spectrum in Fig. 2G and H show the elements information of PANI-HNTs and PB-PANI-HNTs respectively. A dramatic growth in the intensity of Fe and C, N confirms the formation of prussian blue on PANI-HNTs.

Fig. 3

FTIR spectra were also used to further understand the formation of the nanocomposites. Fig. 3 shows the FTIR spectrum of HNTs (a), HNTs-PANI (b) and PB-PANI-HNTs (c). The obvious absorption peaks emerged at 1106 cm^{-1} and 1029 cm^{-1} on the spectrum of HNTs (curve a) are in accordance with the in-plane stretching of Si–O. The characteristic peaks at 1630 cm^{-1}, 3621 cm^{-1} and 3696 cm^{-1} are attributed to the deformation of water, O–H stretching of inner hydroxyl groups and O–H stretching of inner-surface hydroxyl groups, respectively[29]. The new peaks detected at 1301 cm^{-1}, 1486 cm^{-1}, and 1562 cm^{-1} in curve b are ascribed to the vibration of C–C, C=C, and C=N, respectively. In addition, it cannot be ignored that there is a significant shift of the two peaks of Si-O, which also implies the successful polymerization of aniline. In curve c, the absorption band at 2083 cm^{-1} is the main characteristics of Prussian Blue and its analogues, corresponding to the stretching vibration of the C=N group, and the absorption band at 504 cm^{-1} is due to the formation of M–CN–M', indicating the presence of PB. In addition, the absorption bands near 3386 and 1610 cm^{-1} refer to the O–H stretching mode and H–O–H bending mode, respectively, indicating the existence of the interstitial water in the sample.[30-31]

3.2. Electrochemical properties of the PB-PANI-HNT/GCE

Fig. 4

Cyclic voltammetry (CV) is a powerful method in the investigation of electrochemical modification of electrodes and has been used in the present study. Fig. 4A and the inset show the cycle votammogram comparison of different modified electrode. Almost no electrochemical response is observed for the bare glassy carbon electrode (curve d) HNTs (curve c) as the lack of electron mediator. Compared with the bare electrode, the background current of PANI-HNTs (curve d) modified electrode was apparently larger, suggesting that an effective electrode surface area was significantly enhanced due to the use of PANI-HNTs. The CV curve of PANI presents a pair of redox peaks near 0.2 V which is related to two redox processes: leucoemeraldine to emeraldine salt and emeraldine salt to the pernigraniline state. While two pair of well-defined redox couple can be distinguished in curve (b) with potentials located at +0.2 V (peak I) and +0.9 V (peak II) can be seen in PB-PANI-HNTs and PB modified electrode, which related to the PB reduction to Prussian white (PW) and its oxidation to Berlin green (BG) processes, these results are in good agreement with those reported previously.[32-33] The peak separation of PB-PANI-HNTs was valued to be 61 mV and reduction-to-oxidation peak current ratio (Ip_c/Ip_a) was 1.20 at the potential +0.2 V, elucidating high conductivity of the film and reversibility of the redox reaction occurred at the modified surface and also comparable to the previous report.[34] We can also note that the peak current of the PB-PANI-HNTs electrode is higher than that of the PB electrode, and this may attribute to the synergistic effect of PANI-HNTs and PB which could the accelerated the electron transfer and increase the effective area thus enhancing the loading of the PB.

Fig. 4B shows the corresponding CVs of different scan rates ranging from 0.01 V/s to 0.2 V/s limited to the redox reaction region of potential +0.206/0.148 V. Obviously, with the increase of scan rates, the cathodic peak shows gradually negative shift while the anodic peak shows positive shift. The peak current increased linearly with the square root of scan rate (Fig. 4C), and the value of its correlation coefficient R reaches 0.9997 and 0.9998 respectively, which indicating a diffusion-controlled process.

Fig. 5

The stepwise construction process of the sensor was characterized by an electrochemical impedance spectrum (EIS). Nyquist plot of the EIS includes a semicircular portion and a linear portion. The diameter of the semicircle is at higher frequencies correspond to the electron transfer resistance (R_{et}), which shows the electron transfer kinetics of the redox probe. Meanwhile, the linear part at lower frequencies corresponds to the diffusion process. Fig. 5 shows the nyquist plots of various modified electrodes including bare glassy carbon (GC, curve a), HNT (curve b), and PANI-HNTs (curve c), PB-PANI-HNTs (curve d). The EIS of the bare GCE displayed quite small semicircle diameters, implying low resistance (R_{et}) to the redox probe in electrolyte solution. While the value of R_{ct} increased after the HNTs were modified on the glassy carbon electrode, this may ascribed to the less-conductive HNTs. Howerver, the R_{et} of PANI-HNTs is decreased gradually which attribute to the facts that PANI can promote electron transfer. After PB electrodeposited on PANI-HNTs, R_{et} increased a little because the formed PB membrane prevented the electron transfer. All this proved that the PANI-HNTs nanocomposites could act as an excellent electronic substrate and could contribute to much larger response surface and electron transfer passages.

3.3. Electrocatalytic reduction of H_2O_2 at the PB-PANI-HNTs/GCE electrode

Fig. 6

It's well known that the reduced form of PB exhibits a high catalytic activity in the reduction of H_2O_2. So the electrocalytic behavior of the as-prepared PB-PANI-HNTs/GCE modified electrode was investigated in the presence as well as absence of different concentration of H_2O_2. Fig. 6A shows the cyclic voltammograms of the PANI-HNTs/GCE electrode in the presence (d) and PB-PANI-HNTs/GCE in the absence (a) and presence (b, c) of different concentration hydrogen peroxide in 0.1 M buffer solution (pH 7.0) containing 0.1 M KCl. When gradually adding H_2O_2, the

reduction peak current decreased obviously, this well indicated the electrocatalytic reduction and catalytic properties of the modified electrode toward H_2O_2. Meanwhile, the catalytic properties of PB/GCE were also studied as shown in Fig. 6B. The comparison of Fig. 6A and B can well illustrated that PANI coated HNTs can advance the catalytic properties of PB-based sensors, which may be due to the high surface-to-volume ratio with more electroactive sites on PANI-HNTs for H_2O_2 molecules to adsorb and react, and also prove that the presence of PANI-HNTs improved the electron-transfer and enhanced the loading of the PB. The mechanism of the electrocatalytic process can be well shown as follows:[35]

$$Fe_4[Fe(CN)_6]_3+4K^++4e^-\rightarrow K_4Fe_4[Fe(CN)_6]_{3(PW)} \quad (1)$$

$$K_4Fe_4[Fe(CN)_6]_3+2H_2O_2+4H^+\rightarrow Fe_4[Fe(CN)_6]_3(PB)+4OH^-+4K^+ \quad (2)$$

$$H_2O_2 + 2e^- \rightarrow 2OH^- \quad (3)$$

3.4 Amperometric studies：

Fig. 7

The amperometric response of the target sensor toward successive addition of H_2O_2 to a continuously stirring buffer solution was investigated under the optimized conditions (0.1 M PBS, pH 7.0, applied potential of 0 V vs.SCE) as Fig. 7 shows. It was observed that the response time was very fast and the current value reached 95% steady-state response within 3 s. Moreover, a well-defined response was observed during the stepwise increasing of H_2O_2 concentration. The inset shows the linear response of catalytic current to the concentration of H_2O_2 in the range 4 μM to 1064 μM with a linear regression equation expressed as I (μA)=0.0692C(μM) +2.663, and the correlation coefficient is 0.9988. Then the sensitivity and detection limit and was valued to be 0.98 μA/ (μM cm^2) and 0.226 μM (signal-to-noise ratio of 3) respectively. The further comparison of the performance

for H_2O_2 sensing of the target sensor with other H_2O_2 sensors was listed in Table 1. The comparable performance demonstrated that our sensor based on PB-PANI-HNTs modified GCE can be used for the H_2O_2 sensors fabrication.

Table 1

3.5 Effect of Electroactive Interferences

Fig. 8

The influence of typical interfering substances such as glucose (Glu) ascorbic acid (AA), dopamine (DA), was studied. As shown in Fig. 8, 20 μM H_2O_2, 2.0 mM glucose (Glu), ascorbic acid (AA), dopamine (DA) were added into the stirring PBS respectively at a working potential of 0 V. There just showed obvious amperometric response when H_2O_2 were injected, however, the current responses generated due to these interfering species are negligible, indicating that PB-PANI-HNTs/GCE had a superior selectivity to H_2O_2 and it may be attributed to the low potential (0.0 V) employed for the electrocatalysis of H_2O_2 reduction promoted by the PB-PANI-HNTs layer.

3.6 Stability and reproducibility Study of the composite film modified electrode.

Fig. 9

Furthermore, we studied the amperometric response of the PB-PANI-HNTs 0.1 M PBS (pH 7.0) containing 50 μM H_2O_2 under stirred conditions with an applied potential 0 V. Fig. 9A shows the amperometric response of the modified electrode towards the sensing of 50 μM H_2O_2 under continuous stirring condition in 0.1 M PBS for 40 min, it can be seen obviously that the current line remained stable during the experiment, indicating the sensing stability of the PB-PANI-HNTs for the determination of H_2O_2. In addition, the amperometric response over a longer storage period (3 weeks) was also investigate as shown in Fig. 9B, the sensor retained more than 90% of its original sensitivity

in three weeks. This satisfactory performance of the sensor was most likely facilitated by the combination of PB with the PANI-HNTs, which effectively prevented PB leakage from the electrode. The reproducibility of H_2O_2 sensor construction was estimated from the response to 0.5 mM H_2O_2 at five different target electrodes. The results revealed that the electrode possessed satisfied reproducibility with a R.S.D. of 4.7%. Therefore, the modified GCE possessed acceptable repeatability and good stability.

3.7 Real sample analysis

Table 2

The constructed, novel sensor was applied for the analysis of H_2O_2 in tap water with the standard addition method under optimized conditions. The results are illustrated in **Table 2**. Obviously, the recoveries from 96.4% to 99.3% (>90%) acquired were satisfactory, conforming that the potential application of our method in real samples.

4. Conclusion

We presented in this work a new H_2O_2 sensor based on PB-PANI-HNTs composite, which involves one-step in situ polymerization as well as a facial and controllable method electrodeposition. Nonenzymatic and no requirements for linking reagents make it a more accessible method. The PANI-HNTs act as not only the carrier of the active components but also contributes a lot to the activity of the nanoparticles, and this realized highly efficient deposition of PB on the designed electrode. The electrochemical study results indicated the employ of PANI-HNTs well advanced the stability and electrochemical performance of H_2O_2 sensors. Compared with the known amperometric detection of H_2O_2, the PB-PANI-HNTs modified GCE shows faster response, wider linear range, lower detection limit and high stability. At last, the modified GCE can also be used to develop into

biosensor for detection of glucose or other substances which peroxidase catalyzed reactions have H_2O_2 as a by-products and further work is in progress.

Acknowledgements

The authors gratefully acknowledge the financial support of this project by the National Science Fund of China (No. 21275116), Specialized Research Fund for the Doctoral Program of Higher Education (No. 20126101120023), the Natural Science Fund of Shaanxi Province in China (No. 2012JM2013, 2013JM2006 and 2013KJXX-25), the Fund of Shaanxi Province Educational Committee of China (No. 12JK0576), the Scientific Research Foundation of Shaanxi Provincial Key Laboratory (No. 2010JS088, 11JS080, 12JS087, 13JS097).

References:

1 X.L. Luo, J.J. Xu, W. Zhao, H.Y. Chen, A novel glucose ENFET based on the special reactivity of MnO_2 nanoparticles, Biosens. Bioelectron, 2004, 19,1295

2 X. Cui, G. Liu, Y. Lin, Biosensors based on carbon nanotubes/nickel hexacyanoferrate/ glucose oxidase nanocomposites, J. Biomed. Nanotechnol, 2005, 1,320.

3 Q.M. Wang, H.L. Niu, C.J. Mao, J.M. Song, S.Y. Zhang, Facile synthesis of trilaminar core-shell Ag@C@Ag nanospheres and their application for H_2O_2 detection, Electrochim. Acta, 2014, 127, 349.

4 X.H. Shu, Y. Chen, H.Y. Yuan, S.F. Gao, D. Xiao, H_2O_2 Sensor Based on the Room-Temperature Phosphorescence of Nano TiO_2/SiO_2 Composite, Anal. Chem, 2007, 79, 3695.

5 M.C.Y. Chang, A. Pralle, E.Y. Isacoff, C.J. Chang, A selective, cell-permeable optical probe for hydrogen peroxide in living cells, J. Am. Chem. Soc, 2004, 126, 15392.

6 N.V. Klassen, D. Marchington, H.C.E. McGowan, H_2O_2 Determination by the I_3- Method and by $KMnO_4$ Titration, Anal. Chem, 1994, 66, 2921.

7 B. Tang, L. Zhang, K.H Xu, FIA–near-infrared spectrofluorimetric trace determination of hydrogen peroxide using tricarchlorobocyanine dye (Cy.7.Cl) and horseradish peroxidase (HRP), Talanta, 2006, 68, 876.

8 S.X. Xu, J.L. Li, Z.L. Zhou, C.X. Zhang, A third-generation hydrogen peroxide biosensor based on horseradish peroxidase immobilized by sol–gel thin film on a multi-wall carbon nanotube modified electrode, Anal. Methods, 2014, 6, 6310.

9 K. Zhan, H.L. Liu, H. Zhang, Y.L. Chen, H.M. Ni, M. Wu, D.M. Sun, Y. Chen, A facile method for the immobilization of myoglobin on multi-walled carbon nanotubes: Poly(methacrylic acid-co-acrylamide) nanocomposite and its application for direct bio-detection of H_2O_2, J. Electroanal. Chem, 2014, 724, 80.

10 F. Herren, P. Fischer, A. Ludi, W. Haelg, Neutron diffraction study of Prussian blue, $Fe_4[Fe(CN)_6]_3.xH_2O$. Location of water molecules and long-range magnetic order, Inorg. Chem, 1980, 19, 956.

11 D. Moscone, D. D'Otavi, D. Compagnone, G. Palleschi, A. Amine, Construction and Analytical Characterization of Prussian Blue-Based Carbon Paste Electrodes and Their Assembly as Oxidase Enzyme Sensors, Anal. Chem, 2001, 73, 2529.

12 A. A. Karyakin, E. E. Karyakina, L. Gorton, Prussian-Blue-based amperometric biosensors in flow-injection analysis, Talanta, 1996, 43, 1597.

13 P. A. Fiorito, S. I. C. Torresi, Hybrid nickel hexacyanoferrate/polypyrrole composite as mediator hydrogen peroxide detection and its application in oxidase-based biosensors, J. Electroanal. Chem, 2005, 581, 31.

14 E. Nossol, A. J. G. Zarbin, A Simple and Innovative Route to Prepare a Novel Carbon Nanotube/Prussian Blue Electrode and its Utilization as a Highly Sensitive H_2O_2 Amperometric Sensor, Adv. Funct. Mater, 2009, 19, 3980.

15 Y. Zhang, H. Luo, N. Li, Hydrogen peroxide sensor based on Prussian blue electrodeposited on (3-mercaptopropyl)-trimethoxysilane polymer-modified gold electrode, Angew. Chem. Int. Edit, 2011, 34, 215.

16 J. Qiu, H. Peng, R .Liang, J. Li, X. Xia, Synthesis, Characterization, and Immobilization of Prussian Blue-Modified Au Nanoparticles: Application to Electrocatalytic Reduction of H_2O_2, Langmuir, 2007, 23, 2133.

17 T. Uemura, S. Kitagawa, Prussian Blue Nanoparticles Protected by Poly(vinylpyrrolidone), J. Am. Chem. Soc, 2003, 125, 7814.

18 X.L. Zhang, C.H. Sui, J. Gong*, R. Yang, Y.Q. Luo, L.Y. Qu, Preparation, characterization, and property of polyaniline/Prussian blue micro-composites in a low-temperature hydrothermal process Appl. Surf. Sci, 2007, 253, 9030.

19 B. Haghighi, S. Varma, F.M. Alizadeh Sh, Y. Yigzaw, L. Gorton, Prussian blue modified glassy carbon electrodes—study on operational stability and its application as a sucrose biosensor, Talanta, 2004, 64, 3.

20 F. Ricci, G. Palleschi, Sensor and biosensor preparation, optimisation and applications of Prussian Blue modified electrodes, Biosens Bioelectron**,** 2005, 21, 389.

21 W. Jiang, R. Yuan, Y. Q. Chai, B. Yin, Amperometric immunosensor based on multiwalled carbon nanotubes/Prussian blue/nanogold-modified electrode for determination of α-fetoprotein, Anal Biochem, 2010, 407, 65.

22 S. Husmann, E. Nossol, A. J. G. Zarbin, Carbon nanotube/Prussian blue paste electrodes: Characterization and study of key parameters for application as sensors for determination of low concentration of hydrogen peroxide, Sens. Actuators B, 2014, 192, 782.

23 Rawtani, D., Agrawal, Y. K, Rev. Multifarious applications of halloysite nanotubes: a review, Rev Adv Mater Sci, 2012, 30, 282.

24 B. Lecouvet, M. Sclavons and S. Bourbigot, et al., Waterassisted extrusion as a novel processing route to prepare polypropylene/halloysite nanotube nanocomposites: structure and properties, Polymer, 2011, 52, 4284,

25 Yuan, P., Southon, P.D., Liu, Z.W., Green, M.E.R., Hook, J.M., Antill, S.J., Kepert, C.J., Functionalization of Halloysite Clay Nanotubes by Grafting with γ-Aminopropyltriethoxysilane, J. Phys. Chem. C, 2008, 112, 15742.

26 R.C. Liu, B. Zhang, D. D. Mei, et al., Adsorption of methyl violet from aqueous solution by halloysite nanotubes, Desalination, 2011, 268, 11,

27 P.M. Nia, F. Lorestani, W.P. Meng, Y. Alias, A novel non-enzymatic H_2O_2 sensor based on polypyrrole nanofibers–silver nanoparticles decorated reduced graphene oxide nano composites, Appl. Surf. Sci. 2015, 332, 648.

28 A.A. Karyakin, E.E. Karyakina, L. Gorton, On the mechanism of H_2O_2 reduction at Prussian Blue modified electrodes, Electrochem. Commun, 1999, 1, 78.

29 P. Wang , M.L. Du, M. Zhang, H. Zhu, S.Y. Bao, M.L. Zou, T.T. Yang, Facile fabrication of AuNPs/PANI/HNTs nanostructures for high-performance electrochemical sensors towards hydrogen

peroxide CHEM ENG J, 2014, 248, 307.

30 L.F. Lin, X.J. Huang, L.S. Wang, A.M. Tang, Synthesis, characterization and the electrocatalytic application of prussian blue/titanate nanotubes nanocomposite, Solid State Sciences, 2012, 12, 1764.

31 G. Zhao, J.J. Feng, Q.L Zhang, S. P. Li, H.Y. Synthesis and Characterization of Prussian Blue Modified Magnetite Nanoparticles and Its Application to the Electrocatalytic Reduction of H_2O_2, Chem. Mater, 2005, 17, 3154.

32 W. Zhao, J. J. Xu, C. G. Shi, H. Y. Chen, Multilayer Membranes via Layer-by-Layer Deposition of Organic Polymer Protected Prussian Blue Nanoparticles and Glucose Oxidase for Glucose Biosensing, Langmuir, 2005, 21, 9630.

33 S. Q. Liu, J. J. Xu, H. Y. Chen, Electrochemical behavior of nanosized Prussian blue self-assembled on Au electrode surface, Electrochem. Commun, 2002, 4, 421.

34 H. Razmi, R. Mohammad-Rezaei, H. Heidari, Self-Assembled Prussian Blue Nanoparticles Based Electrochemical Sensor for High Sensitive Determination of H_2O_2 in Acidic Media, Electroanalysis, 2009, 21, 2355.

35 T. Uemura, M. Ohba, S. Kitagawa, Size and Surface Effects of Prussian Blue Nanoparticles Protected by Organic Polymers, Inorganic Chemistry, 2004, 43, 7339.

36 M. Gaitán, V.R. Goncales, G. Soler-Illia, L.M. Baraldo, S.I. Córdoba de Torresi., Structure effects of self-assembled Prussian blue confined in highly organized mesoporous TiO_2 on the electrocatalytic properties towards H_2O_2 detection, Biosens**.** Bioelectron, 2010, 26, 890.

37 J.H. Yang, Noseung Myoung, H.G. Hong, Facile and controllable synthesis of Prussian blue on chitosan-functionalized graphene nanosheets for the electrochemical detection of hydrogen peroxide, Electrochim Acta, 2012, 81, 37.

38 L. Wang, Y.J. Ye, H.Z. Zhu, Y. H. Song, S. J. He, F.G. Xu, H.Q. Hou, Controllable growth of Prussian blue nanostructures on carboxylic group-functionalized carbon nanofibers and its

application for glucose biosensing, Nanotechnology, 2012, 23, 455502.

39 E. Jin, X.F. Lu, L.L. Cui, D.M. Chao, C. Wang, Fabrication of graphene/prussian blue composite nanosheets and their electrocatalytic reduction of H_2O_2, Electrochim. Acta, 2010, 55, 230.

40 A.H. Keihana, S. Sajjadic, Improvement of the electrochemical and electrocatalytic behavior of Prussian blue/carbon nanotubes composite via ionic liquid treatment, Electrochimi. Acta, 2013, 113, 803.

FIGURES AND CAPTIONS

Fig. 1 Schematic illustration of the fabrication of PB-PANI-HNTs film and electrocatalytic mechanism of PB-PANI-HNTs modified electrode.

Fig. 2 TEM of HNTs (A, B), PANI-HNTs (C, D) and PB-PANI-HNTs (E, F) and EDS analyses of PANI-HNTs (G) and PB-PANI-HNTs (H) nanohybrid films.

Fig. 3 FTIR spectra of (a) HNTs (b) PANI-HNTs and (c) PB-PANI-HNTs nanocomposites.

Fig. 4 (A) Cyclic voltammograms of the (a) PANI-HNTs/GCE (b) PB-PANI-HNTs/GCE and the inset (c) PANI-HNTs/GCE (d) GCE (e) HNTs/GCE in 0.1 M KCl solution an the scan rate of 50 mV/s. (B) Cyclic voltammograms corresponding to the PB-PANI-HNT s/GCE in 0.1 M KCl at scan rate of 0.01, 0.02, 0.04, 0.06, 0.08, 0.1, 0.12, 0.14, 0.18 and 0.2 V/s (from inside to outside). (C) The plot of anodic and peak currents *vs*. square root of scan rate.

Fig. 5 EIS of bare glassy carbon (a), HNT (b), and PANI-HNTs composite (c), PB-PANI-HNTs (d) modified electrodes in 5.0 mM $[Fe(CN)6]^{4-/3-}$ containing 0.1 M KCl from 10^5 to 10^{-2} Hz at amplitude

of 5 mV.

Fig. 6 (A) Cyclic voltammograms of PB-PANI-HNTs/GCE in the absence (curve a) and presence (curve b, c) of 0.3 mM, 1.2 mM H_2O_2, and PANI-HNTs/GCE in the presence of 1.2 mM H_2O_2 (curve d) (B) PB/GCE in the absence (curve a') and presence (curve b', c') of 0.3 mM, 1.2 mM H_2O_2 0.1 M buffer solution (pH 7.0) containing 0.1 M KCl.

Fig. 7 (A) Amperometric response of PB-PANI-HNTs/GCE after successive addition of H_2O_2 into a 0.1 M PBS (pH 7.0) with continuously stirring, applied potention 0 V. The inset shows the corresponding calibration curve for PB-PANI-HNTs modified electrode.

Fig. 8 Amperometric response of PB-PANI-HNTs/GCE after adding 20 μM H_2O_2, (2 mM) Glu, AA, and AP.

Fig. 9 (A) The long-term stability response of PB-PANI-HNTs/GCE towards the sensing of 50 μM H_2O_2 under continuous stirring condition in 0.1 M PBS containing 0.1 M KCl for 40 min. (B) Long-term stability study of the PB-PANI-HNTs/GCE sensor. Each data represents the current response of the sensor to addition of 50 μM H_2O_2. (Applied potention: 0 V) The response is normalized with respect to the response on the first day.

Table 1 Electroanalytical characteristics of various modified electrodes toward H_2O_2

Table 2 Determination of hydrogen peroxide in tap water

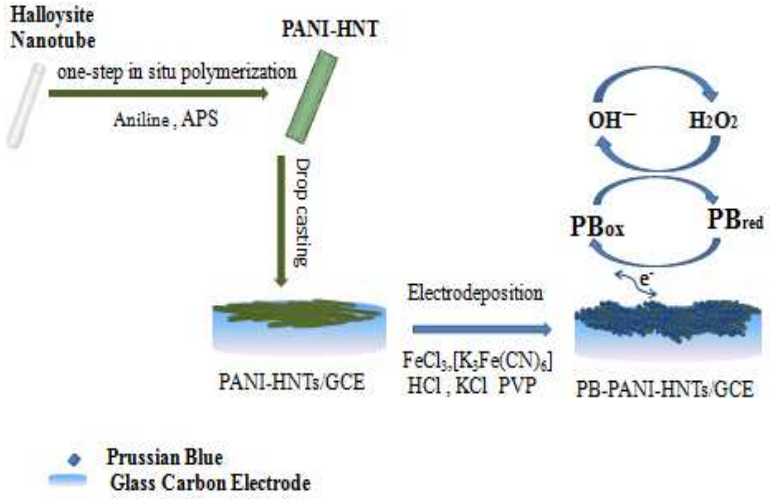

Fig. 1 Schematic illustration of the fabrication of PB-PANI-HNTs film and electrocatalytic mechanism of PB-PANI-HNTs modified electrode.

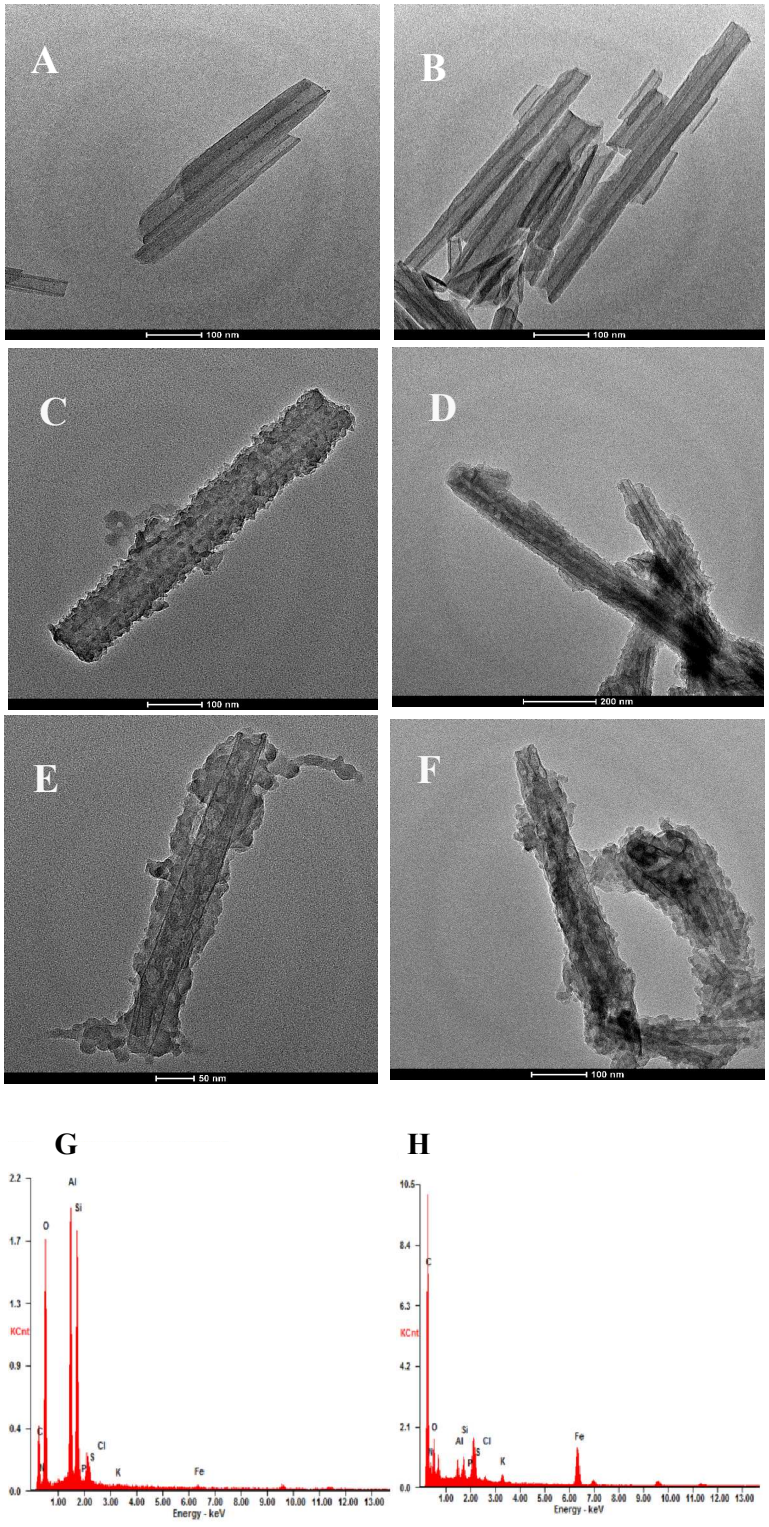

Fig. 2 TEM of HNTs (A, B), PANI-HNTs (C, D) and PB-PANI-HNTs (E, F) and EDS analyses of PANI-HNTs (G) and PB-PANI-HNTs (H) nanohybrid films.

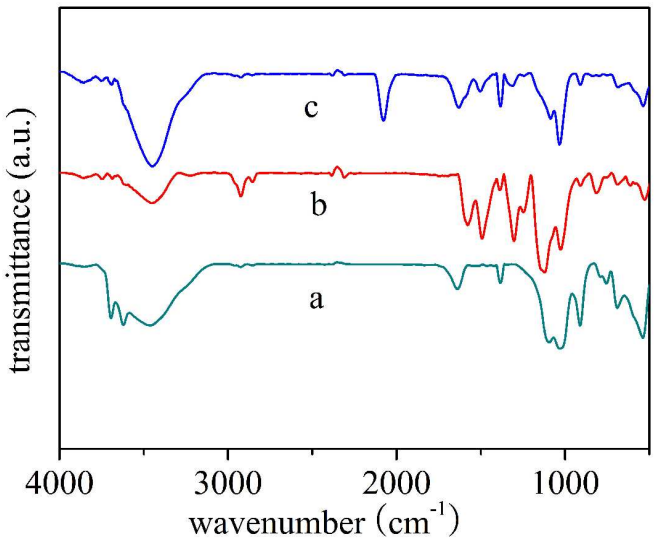

Fig. 3 FTIR spectra of (a) HNTs (b) PANI-HNTs and (c) PB–PANI–HNTs nanocomposites.

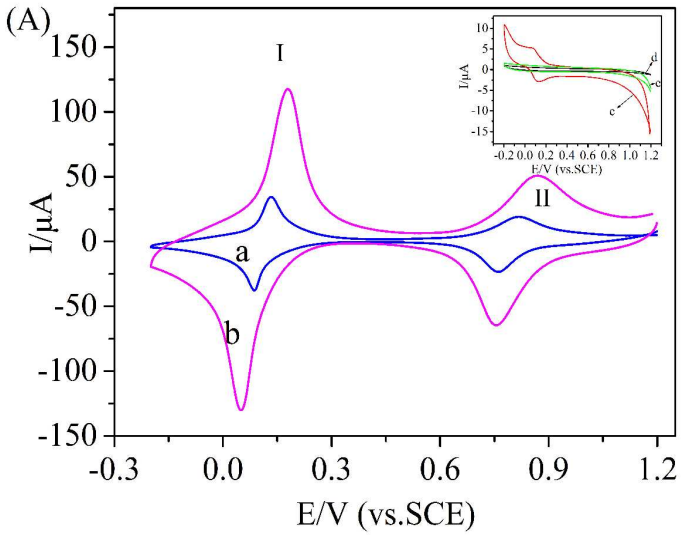

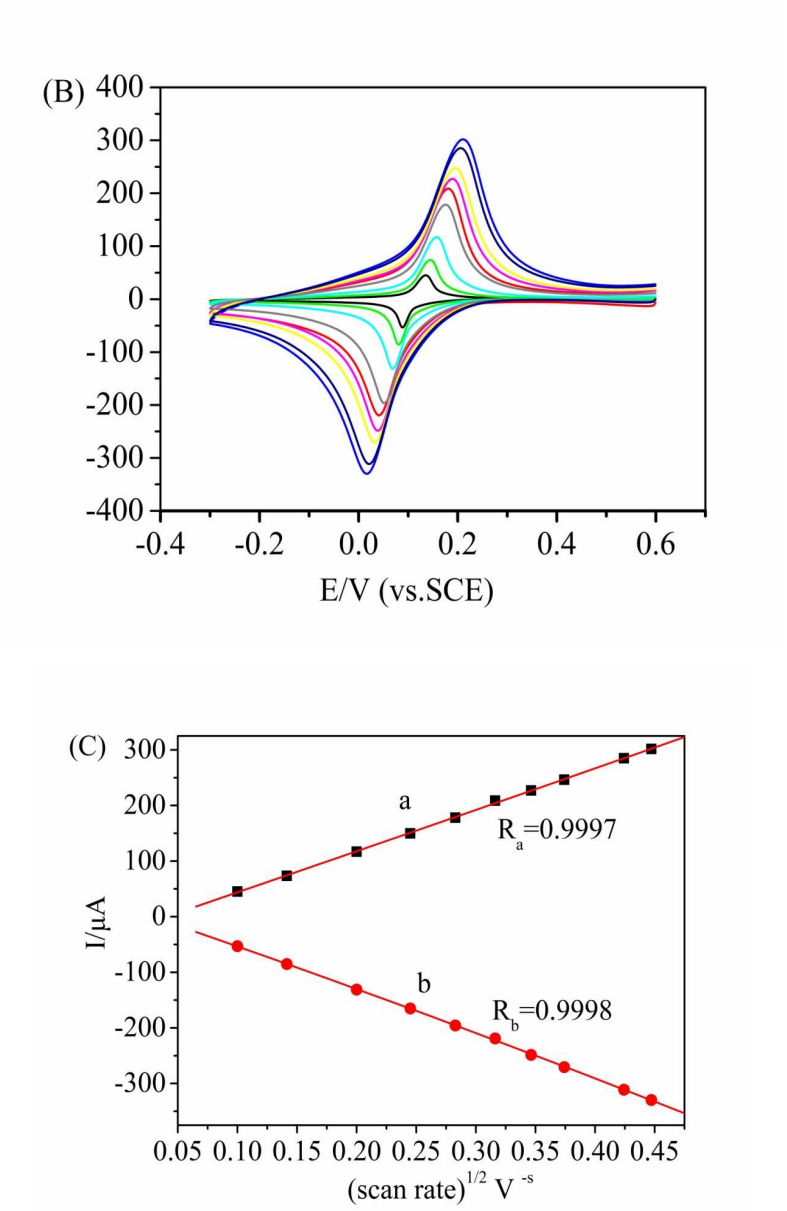

Fig. 4 (A) Cyclic voltammograms of the (a) PANI-HNTs/GCE (b) PB-PANI-HNTs/GCE and the inset (c) PANI-HNTs/GCE (d) GCE (e) HNTs/GCE in 0.1 M KCl solution an the scan rate of 50 mV/s. (B) Cyclic voltammograms corresponding to the PB-PANI-HNTs/GCE in 0.1 M KCl at scan rate of 0.01, 0.02, 0.04, 0.06, 0.08, 0.1, 0.12, 0.14, 0.18 and 0.2 V/s (from inside to outside). (C) The plot of anodic and peak currents *vs*. square root of scan rate.

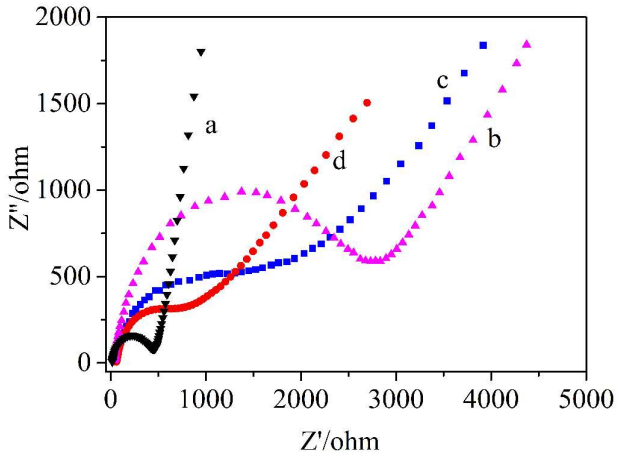

Fig. 5 EIS of bare glassy carbon (a), HNT (b), and PANI-HNTs composite (c), PB-PANI-HNTs (d) modified electrodes in 5.0 mM $[Fe(CN)6]^{4-/3-}$ containing 0.1 M KCl from 10^5 to 10^{-2} Hz at amplitude of 5 mV.

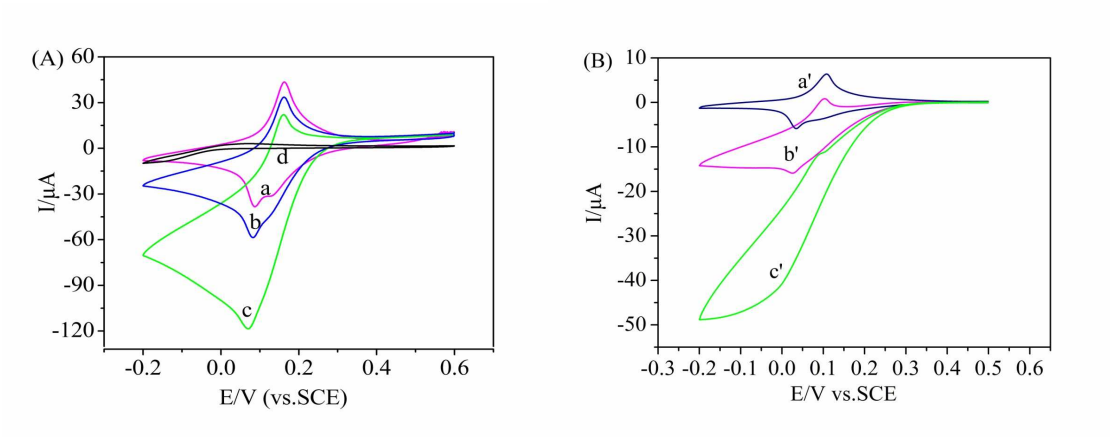

Fig. 6 (A) Cyclic voltammograms of PB-PANI-HNTs/GCE in the absence (curve a) and presence (curve b, c) of 0.3 mM, 1.2 mM H_2O_2, and PANI-HNTs /GCE (curve d) in the presence of 1.2 mM H_2O_2. (B) PB/GCE in the absence (curve a') and presence (curve b', c') of 0.3 mM, 1.2 mM H_2O_2 in 0.1 M buffer solution (pH 7.0) containing 0.1 M KCl.

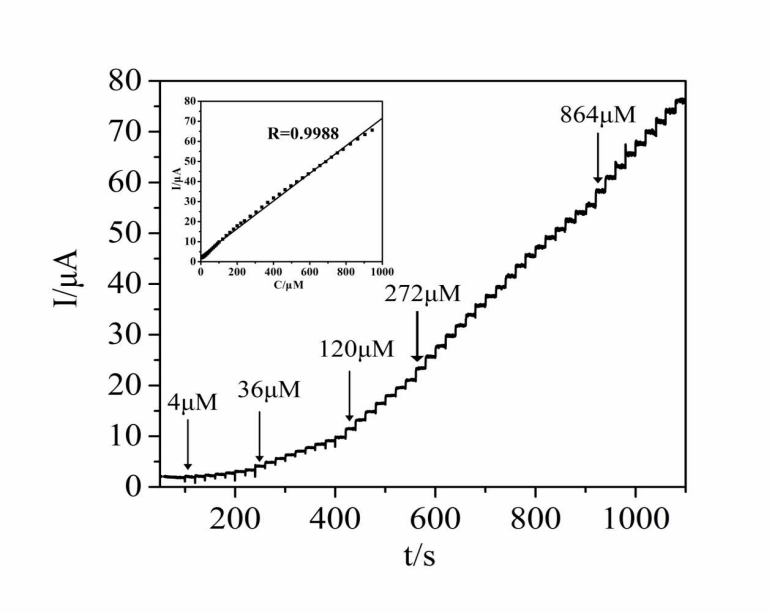

Fig. 7 (A) Amperometric response of PB/GCE after successive addition of H_2O_2 into a 0.1 M PBS (pH 7.0) containing 0.1 M KCl with continuously stirring, applied potention: 0 V. The inset shows the corresponding calibration curve for PB-PANI-HNTs modified electrode.

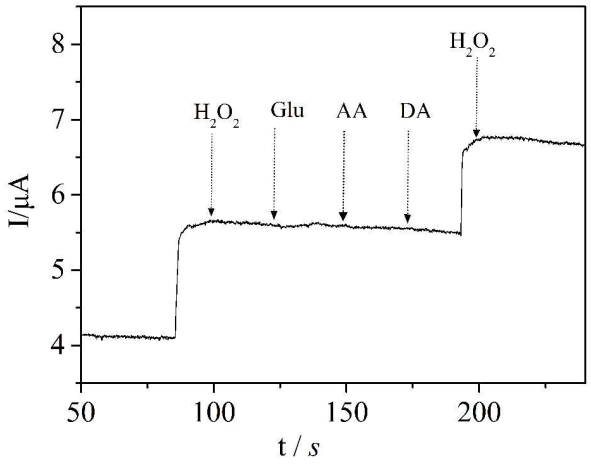

Fig. 8 Amperometric response of PB-PANI-HNTs/GCE after adding 20 μM H_2O_2, (2 mM) Glu, AA, and AP.

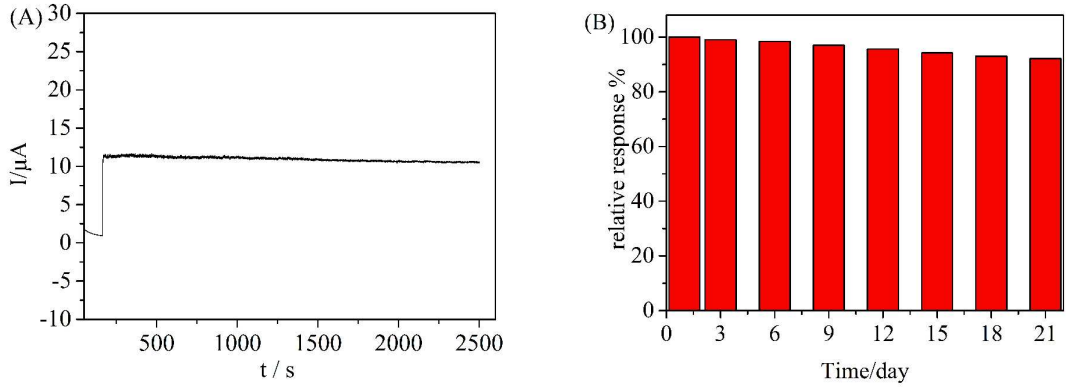

Fig. 9 (A) sensing stability PB-PANI-HNTs/GCE in a stirring PBS solution containing 50 μM H_2O_2 for 40 min at 0 V. (B) Long-term stability study of the PB-PANI-HNTs/GCE sensor. Each data represents the current response of the sensor to addition of 50 μM H_2O_2. (Applied potention: 0 V) The response is normalized with respect to the response on the first day.

Table 1 Electroanalytical characteristics of various modified electrodes toward H_2O_2.

Electrode	Linear range (mM)	Detection limit (μM)	Sensitivity (A/M·cm^2)	Reference
PB-TiO_2/ITO[a]	0.1-1.4	0.42	0.03	36
PB-CS[b]-RGO/GCE	0.01-0.4	0.2	0.86	37
PB-FCNFs/GCE	0.04–25	0.7	0.064	38
PB-RGO[c]/GCE	0.02–0.2	1.9	0.02	39
PB/CNTs/GC	0.004-0.35	4.1	0.101	40
PB-PANI-HNTs/GCE	0.004—1.1	0.226	0.98	This work

a.ITO: Indium tin oxide; b.CS: chitisan; c. RGO: Reduced graphene oxide.

Table 2 Determination of hydrogen peroxide in tap water

Sample no.	H_2O_2 added (μM)	H_2O_2 found (μM)	Recovery (%)	RSD[a](%)

1	50	48.2	96.4	3.7
2	100	98.7	98.7	3.3
3	200	198.6	99.3	2.9

[a] RSD (%) calculated from five measurements.